Synthesis and Characterization of $Zr_2Al_3C_4$ Thin Films

Chung-Chuan Lai[†], Mark D. Tucker[*], Jun Lu, Jens Jensen, Grzegorz Greczynski, Per Eklund, Johanna Rosen

Thin Film Physics Division, Department of Physics, Chemistry and Biology (IFM), Linköping University, SE-581 83 Linköping, Sweden

[*] Current affiliation: Department of Physics and Astronomy, Curtin University, Perth WA 6102, Australia

[†] Corresponding author: Chung-Chuan Lai (E-mail address: chula@ifm.liu.se)

Abstract

$Zr_2Al_3C_4$ is an inherently nanolaminated carbide where layers of ZrC alternate with layers of Al_3C_2. Characterization of bulk samples has shown it has improved damage tolerance and oxidation resistance compared to its binary counterpart ZrC. Though a potential candidate for coatings applied for use in harsh environments, thin films of $Zr_2Al_3C_4$ have not been reported. We have synthesized epitaxial $Zr_2Al_3C_4$ thin films by pulsed cathodic arc deposition from three elemental cathodes, and have studied the effect of incident atomic flux ratio, deposition temperature, and choice of substrate on material quality. X-ray diffraction analysis showed that $Zr_2Al_3C_4$ of the highest structural quality was obtained for growth on 4 H–SiC(001) substrate at 800 °C. Also, suppression of competing phases could be achieved on α-Al_2O_3(001) at elevated substrate temperatures. Very similar growth behavior to that of the well-known $M_{n+1}AX_n$ phases – Al supersaturation, binary carbide intergrowth and high sensitivity to choice of substrate – indicates a strong connection between the two families of materials, despite their differences in structure and in chemistry.

Keywords: Thin film; Cathodic arc deposition; Zr2Al3C4; Nanolaminate; Zirconium carbide

1. Introduction

The binary transition metal carbides (MC, where M is a transition metal) have been thoroughly studied since the 1930s, in part motivated by attention from industry [1]. MCs are generally harder, ore refractory, and more chemically stable than their metallic counterparts, while remaining electrically and thermally conductive, but they are brittle [2]. Today, they are commonly utilized as reinforcement in composites (e.g.WC–Co [3]) and protective coatings (e.g. TiC, NbC, CrC [4]).

In order to improve the performance of binary carbides at elevated temperature, a third component can be introduced, forming ternary transition metal carbides (MAC, where A is typically a group 13–16 element). Commonly, the A element is Al, as in Ti_2AlC, Ti_3AlC_2 and $Zr_2Al_3C_4$, causing improvement in high temperature oxidation resistance by the formation of a continuous and dense oxygen diffusion barrier of alumina on the surface [5–10].

A class of ternary and quaternary carbides have inherently nanolaminated structures with alternating transition metal carbide layers (MC) and A-element-containing layers (A or AC) along one crystal axis [11]. They have several different formulas $M_{n+1}AC_n$, $(MC)_n(A_3C_2)$, and $(MC)_n(A_4C_3)$, where n is 1–3 [12,13], for example Ti_3AlC_2, $(ZrC)_2(Al_3C_2)$ or $Zr_2Al_3C_4$, and $(HfC)_3(Al_4C_3)$ or $Hf_3Al_4C_6$ [14–16]. They commonly have superior mechanical properties, such as higher tolerance against damage and increased machinability, to their binary carbide counterparts [14,17,18].These properties originate from their layered structures.

$Zr_2Al_3C_4$ was first reported in bulk form in 1980 by Schuster and Nowotny [19], but detailed studies on properties of this phase were not conducted until the 2000s. The material exhibits high electrical conductivity ($1.10\ \mu\Omega m$) along with higher stiffness and toughness than ZrC [20] and an improved high temperature oxidation resistance. Because of these properties, Zhou et al. proposed

$Zr_2Al_3C_4$ as a potential candidate for applications such as reinforcing composite for metals [21] and protective conducting coatings in harsh environments [13]. However, thin film synthesis of inherently nanolaminated phases in the Zr–Al–C system, including $Zr_2Al_3C_4$, has not yet been reported.

Here, we report synthesis of $Zr_2Al_3C_4$ thin films by pulsed cathodic arc deposition. Samples deposited with different Al to Zr and C to Zr incident atomic flux ratios, on different substrates (α-Al_2O_3(001), MgO(111), 4 H–SiC(001), and yttria-stabilized-zirconia (YSZ) (111)), and at different substrate temperatures (700 °C, 750 °C, 800 °C and 900 °C) were investigated. Epitaxial growth of $Zr_2Al_3C_4$ was achieved on 4 H–SiC substrates, and suppression of competing phases could also be achieved on α-Al_2O_3 at elevated substrate temperatures.

2. Experimental details

2.1 Thin film synthesis

All depositions were made in a high current pulsed cathodic arc system equipped with three cylindrical cathodes (Ø = 25 mm), slightly tilted to allow plasma flux into a copper solenoid filter for macroparticle removal. This method has previously been used for synthesis of laminated carbides [22–24], see Ref. [25] for details about the deposition system. Each cathode is surrounded by a cylindrical anode and is triggered using a center-positioned tungsten trigger pin electrically insulated from the cathode. During deposition, the cathodes are fired separately, at a base pressure of around 10^{-7} mbar.

The samples were deposited from three elemental cathodes, Zr, Al and C, with purities of 99.9%, 99.99% and 99.99%, respectively (*Testbourne Ltd.*), using an arc current of 1.5 kA and a pulsed

frequency of 11 Hz. The width of one pulse for the Zr, Al and C cathodes were 350, 250 and 500 μs, respectively.

The incoming atomic flux ratio was controlled by triggering the three cathodes in a repeating pulse sequence and varying the number of pulses to each cathode in the sequence. In initial calibrations the deposition rate from each cathode was determined by attaining density and thickness from X-ray reflectivity (XRR) measurements on samples deposited on Si(100) substrates at room temperature. This information was used to determine the atomic flux ratio incident on the substrate (or the 'flux ratio') for a chosen pulse sequence.

The substrates used in this work were α-Al_2O_3(001), MgO(111), 4 H–SiC(001), and yttria-stabilized zirconia (111) (YSZ, $Zr_{0.92}Y_{0.08}O_2$). All substrates were cleaned in an ultrasonic bath for 10 min each in acetone then isopropanol, and were blown dry with N_2. The substrate was kept for 15 min at the deposition temperature before material synthesis to ensure a uniform temperature over the sample. One thin film sample, presented in Section 3.1, was deposited on 4 H–SiC(001) with a thickness of about 200 nm for better statistics in composition analysis, see Section 2.2. The other samples presented were about 20 nm thick according to deposition rate calibration prior to the sample deposition.

2.2 Thin film characterization

XRR and X-ray diffraction (XRD) patterns were acquired in an X-ray diffractometer (*Empyrean, PANalytical B.V.*) using CuKα radiation and a Ge(220) crystal hybrid monochromator on the incident side and a parallel plate collimator (PPC) on the receiving side. An extra equatorial 0.1 mm collimator slit was inserted between the PPC and the detector when acquiring XRR patterns, which later were fitted within X'Pert Reflectivity software (Ver. 1.3, *PANalytical B.V.*) to obtain

the density and thickness of the calibration samples. XRD was used for phase identification and analysis of crystal orientation.

The microstructure of the films was characterized using high resolution transmission electron microscopy (HR-TEM) on cross cross sectional samples in a FEI Tecnai G2 microscope operated with an acceleration voltage of 200 kV.

Time-of-flight elastic recoil detection analysis (TOF-ERDA) was performed on the thicker sample to obtain an average composition from a larger sampling volume and a more reliable quantification of the lighter elements, such as C, O and N.

3. Results and Discussion

3.1 Characterization of $Zr_2Al_3C_4$ thin films

Fig. 1(a) is a θ–2θ XRD pattern of a $Zr_2Al_3C_4$ thin film deposited on 4 H–SiC(001) at 800 °C with flux ratio (Al/Zr) = 5.75 and (C/Zr) = 1.67. The six diffraction peaks labeled s in Fig. 1 (a) are the basal planes (00 l) of the SiC substrate [26]. The eight peaks at around 7.9°, 15.9°, 24.2°, 32.3°, 40.7°, 58.4°, 67.7° and 77.3° share the same least common multiple of interplanar spacing (d spacing) ~11.1 Å, and can be assigned to diffraction from the basal planes (00 l) of the $Zr_2Al_3C_4$ phase with a c parameter of ~22.2 Å [27]. The additional peaks at ~33.0° and ~69.1° are the 111 and 222 peaks of cubic ZrC_x ($0.67 \leq x \leq 1.0$) [28]. The inset of Fig. 1(a) is an in-plane ($\psi \sim 90°$) θ–2θ XRD pattern over the range 2θ = 52–62° showing 110 diffraction of $Zr_2Al_3C_4$ and the substrate. From the position of $Zr_2Al_3C_4$(110) its a parameter can be determined to be ~3.34 Å, while the asymmetric shape of the peak indicates an overlap of a ZrC_x 220 peak with lower intensity.

Fig. 1 (b) shows φ-scans acquired at 2θ = 65.702°, 53.040° and 58.560° and at fixed tilt angle ψ from the surface normal of the sample, with ψ = 68.50°, 55.50° and 63.00°, which correspond to
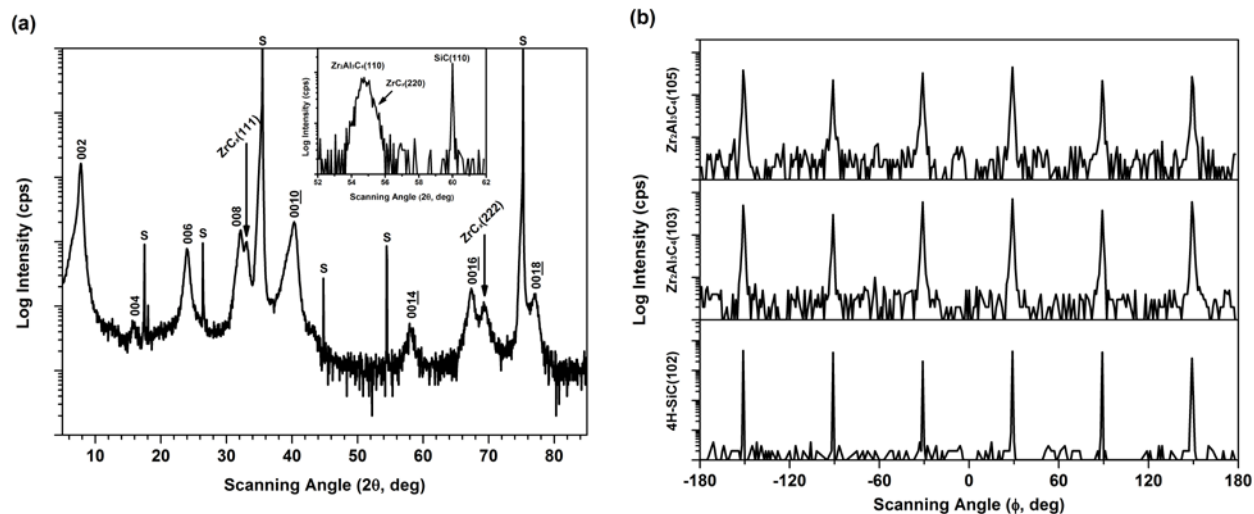
Fig. 1. (a) θ–2θ XRD patterns of a $Zr_2Al_3C_4$ thin film grown on 4 H–SiC(001) at 800 °C. The inset is an in-plane θ–2θ XRD pattern over the range $2\theta = 52$–$62°$. (b) Tilted φ-scan XRD patterns on the $Zr_2Al_3C_4$(103), $Zr_2Al_3C_4$(105) and 4 H–SiC(102) planes of the sample shown in (a).

diffraction from $Zr_2Al_3C_4$(103), $Zr_2Al_3C_4$(105) and 4 H–SiC(102) planes, respectively. The six peaks separated by 60° in all three scans share the same φ peak positions, indicating the epitaxial relation $Zr_2Al_3C_4$[100] || 4 H–SiC[100] and $Zr_2Al_3C_4$[001] || 4 H–SiC[001].

TOF-ERDA quantification of the sample investigated in Fig. 1 showed average atomic concentrations of (Zr, Al, C, O, N) = (29.3, 26.8, 43.1, 0.6, 0.1) at.%, respectively. Traces of Ti and Hf, which are both common impurities found in Zr cathodes [29], were also observed but at levels below the quantification limit. This data shows that, relative to the composition of $Zr_2Al_3C_4$, the film is deficient in Al, explaining the presence of ZrC_x formed from the excess Zr and C. The nearly 4 times higher (Al/Zr) flux ratio than the stoichiometry of $Zr_2Al_3C_4$ phase, as well as the Al deficiency observed in this film, were likely due to high sublimation rate and low sticking

coefficient of Al at 800 °C. The known higher sputter yield of Al compared to C may also lead to a high rate of Al resputtering by the relatively massive Zr species.

Figs. 2 (a) and (b) are TEM images of the sample investigated in Fig. 1, acquired along the [110] zone axis. Fig. 2 (a) shows a layered pattern with a vertical period of ~22.2 Å, which matches with the c lattice parameter of $Zr_2Al_3C_4$. The inset is a SAED pattern acquired along the same zone axis and two diffraction points closest to the origin are indexed. Fig. 2 (b) shows an overview image of the film, where a ZrC_x intergrowth layer can be observed in between a defect-rich $Zr_2Al_3C_4$ layer and a $Zr_2Al_3C_4$ layer with tilted grains. These tilted grains grew on the defect-rich and rough
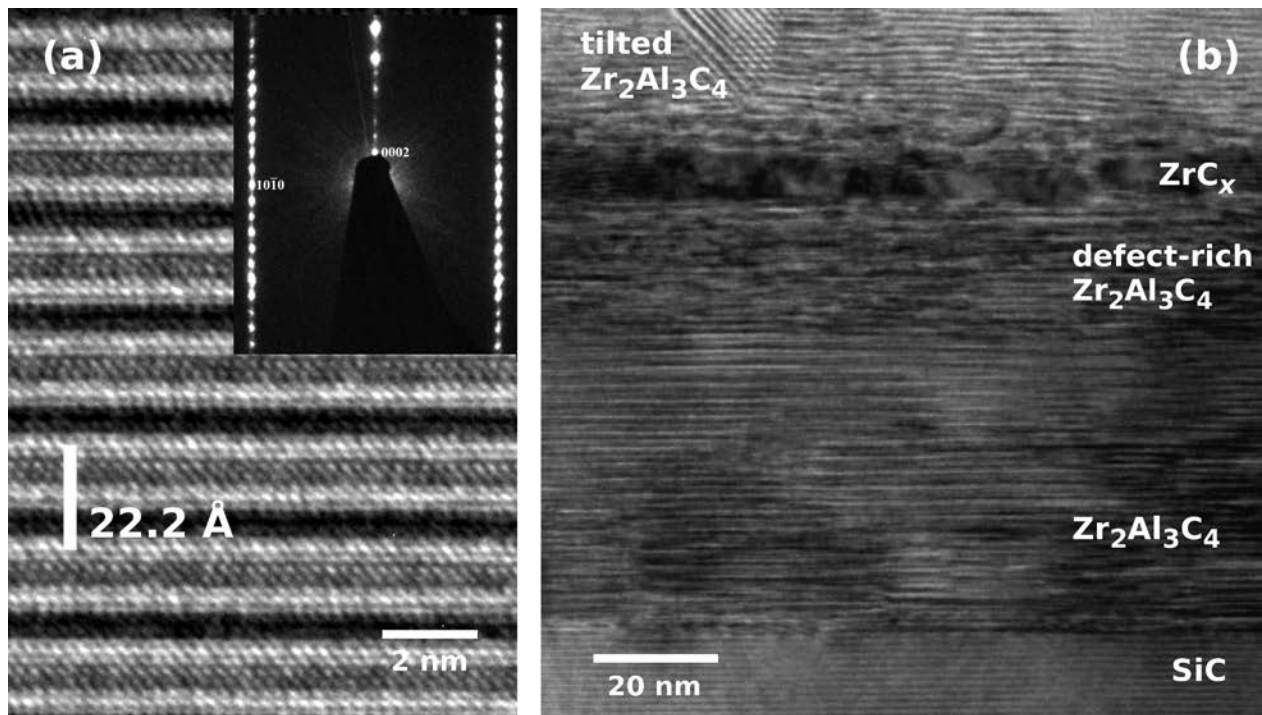
Fig. 2. HR-TEM images acquired along the [110] zone axis of the $Zr_2Al_3C_4$ sample shown in Fig. 1. (a) The multilayer structure of the $Zr_2Al_3C_4$ crystal. The inset is the corresponding SAED pattern. (b) An overview image showing different $Zr_2Al_3C_4$ layers and ZrC intergrowth.

surface of the underlying ZrC_x layer, which promoted the nucleation of other planes than the basal planes, normally the planes with the lowest surface energy. This shows that epitaxy of $Zr_2Al_3C_4$ strongly depends on the structural quality of the surface where nucleation takes place.

Lin et al. have previously observed the intergrowth of ZrC_x phase in $Zr_2Al_3C_4$ and related nanolaminated phases with high-resolution scanning transmission electron microscopy [30]. Similarly, observations of binary carbide intergrowth have been reported in other thin films of layered ternary carbides, for example Ti_2AlC and Ti_3SiC_2, where they were explained by a high sensitivity to local composition changes in such ternary phases [31,32]. Here, the onset of Al deficiency during the deposition can possibly be related to the transition into the defect rich $Zr_2Al_3C_4$ layer. The ZrC_x layer started to nucleate when the Al concentration was too low to form the $Zr_2Al_3C_4$ phase, and the tilted $Zr_2Al_3C_4$ layer started to grow on the ZrC_x layer as Al concentration was increased again.

3.2 Effect of the flux ratio

Fig. 3 (a) shows θ–2θ XRD patterns of three samples grown on α-Al_2O_3(001) with different (Al/Zr) flux ratios. The sharp peaks at 20.5° and 41.7° are α-Al_2O_3 003 and 006 peaks respectively [26]. The peaks from $Zr_2Al_3C_4$ basal planes (at similar positions as in Fig. 1 (a)) are marked with dashed lines and labeled 00 *l*, *l* = 2, 4, 6..., here and in Fig. 3 (b) and 4. The ZrC_x 111 and 222 peaks are again observed at 33.0° and 69.1°. The peaks at 38.0° and 81.0°, sharing a common multiple of *d* spacing ~2.37 Å, are identified as (114) and (228) planes of tetragonal $ZrAl_3$ [33]. The $ZrAl_3$ intermetallic phase is a commonly found phase in the synthesis of Zr–Al–C ternary carbides, such as $Zr_2Al_3C_4$, $Zr_3Al_3C_5$ and $Zr_2Al_4C_5$ [20,34–36].
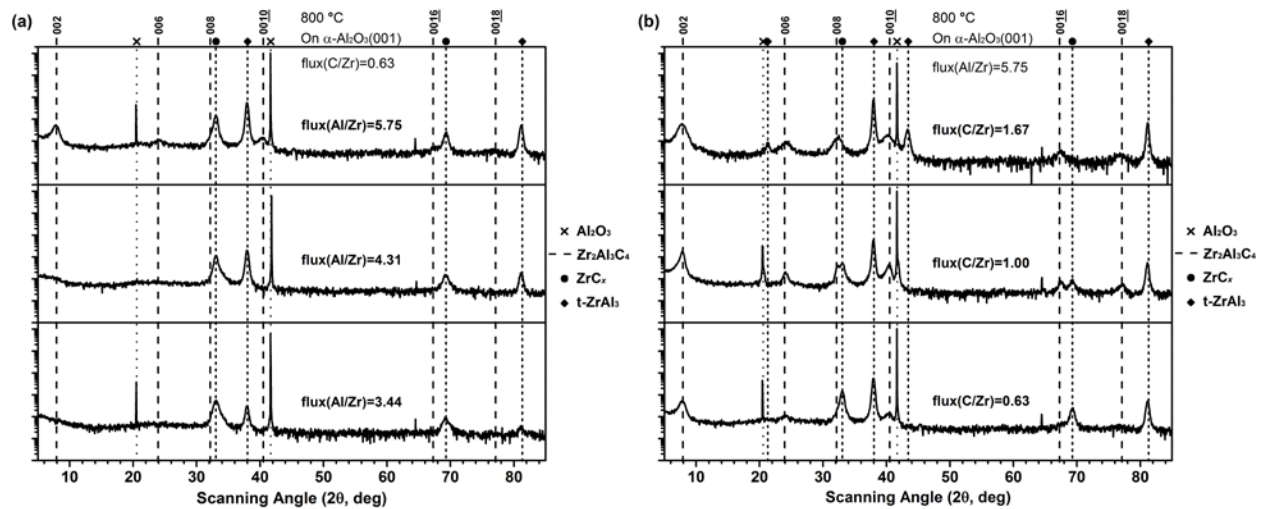
Fig. 3. θ–2θ XRD patterns of $Zr_2Al_3C_4$ grown on α-Al_2O_3(001) at 800 °C with (a) different (Al/Zr) incident atomic flux ratios and (b) different (C/Zr) incident atomic flux ratios.

In Fig. 3 (a), the intensities of the $Zr_2Al_3C_4$ peaks increase with increasing (Al/Zr) flux ratio, which indicates a preferable growth condition for $Zr_2Al_3C_4$ crystals with higher Al flux. It is worth noting that a clear trace of $Zr_2Al_3C_4$ 002 peak appears when the flux ratio (Al/Zr) = 5.75, which is more than 3 times that of (Al/Zr) = 1.50 as in the stoichiometric $Zr_2Al_3C_4$. This is similar to our observation in Section 3.1, where a high or possibly supersaturating Al in the deposition flux is needed for nucleation and growth of $Zr_2Al_3C_4$ phase. When the Al flux is not sufficiently high, ZrC_x starts to nucleate and grow. Again, the supersaturation of the *A* element (Al, Si…etc.) in the ternary carbide systems is often required to initiate the nucleation of the phases [11,31,32]. Notice that the (C/Zr) flux ratio is very close to 0.67 of the Zr_3AlC_2 stoichiometry, though the latter phase has not yet been reported. Even within our tested incident composition range the (Al/Zr) flux ratio varies from 0 to 5.75, no Zr_3AlC_2 phase has been observed.

9

Fig. 3 (b) shows θ–2θ XRD patterns of three samples grown on α-Al$_2$O$_3$(001) with varied (C/Zr) flux ratio, where similar competing phases, ZrC$_x$ and ZrAl$_3$, are observed as in Fig. 3 (a). It shows that the Zr$_2$Al$_3$C$_4$ phase appears for a (C/Zr) flux ratio between 0.63 to 1.67, i.e. from less than 1/3 up to 5/6 of the Zr$_2$Al$_3$C$_4$ stoichiometry. For this wide synthesis window, improved crystal quality can be found when the (C/Zr) flux ratio approaches the ideal stoichiometry, which increases the intensity of diffraction peaks Zr$_2$Al$_3$C$_4$ 008 and 0010. Meanwhile, the decreasing ZrC$_x$ and increasing Zr$_2$Al$_3$C$_4$ intensity indicate that higher C flux stabilizes more Zr in Zr$_2$Al$_3$C$_4$ phase.

In both Figs. 3 (a) and (b), a high (Al/Zr) flux ratio is commonly needed in order to form Zr$_2$Al$_3$C$_4$, also favoring the formation of ZrAl$_3$ phase. The almost unchanged ZrAl$_3$ intensity when varying the C flux, and the increasing ZrAl$_3$ intensity when increasing the Al flux indicates that the Al flux is a more important determinant of the presence of this competing phase. Since Zr$_2$Al$_3$C$_4$ requires higher Al flux ratio to nucleate, it seems difficult to purify the ternary phase simply by varying the incident flux ratio at this temperature.

3.3 Effect of substrate temperature

Fig. 4 shows θ–2θ XRD patterns of samples deposited on α-Al$_2$O$_3$(001) with the same flux ratio, (Al/Zr) = 5.75 and (C/Zr) = 1.67, at temperatures of 700 °C, 750 °C, 800 °C and 900 °C. A very low intensity Zr$_2$Al$_3$C$_4$ 008 peak can be observed at 700 °C, which increases in intensity with increasing substrate temperature. The only competing phase observed is the ZrAl$_3$ phase, which is dominant at lower temperatures. In the sample deposited at 900 °C, the film appears highly phase pure Zr$_2$Al$_3$C$_4$, with no trace of competing phases in the XRD pattern.

The observation of the increased Zr$_2$Al$_3$C$_4$ phase purity at higher temperatures indicates preferred growth of the phase compared to the competing phase, ZrAl$_3$, and is explained by increased adatom
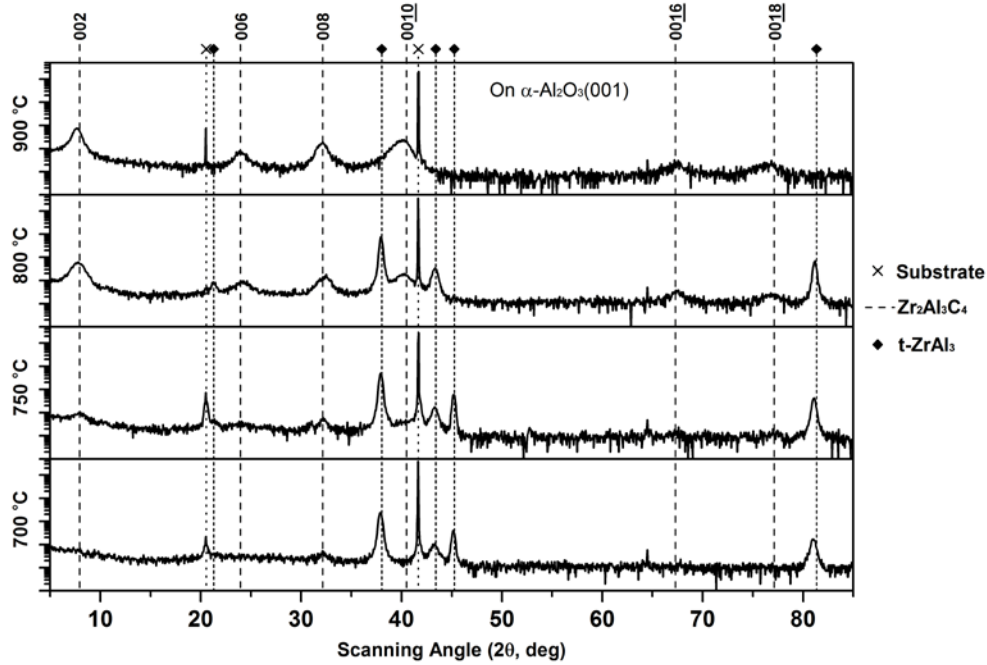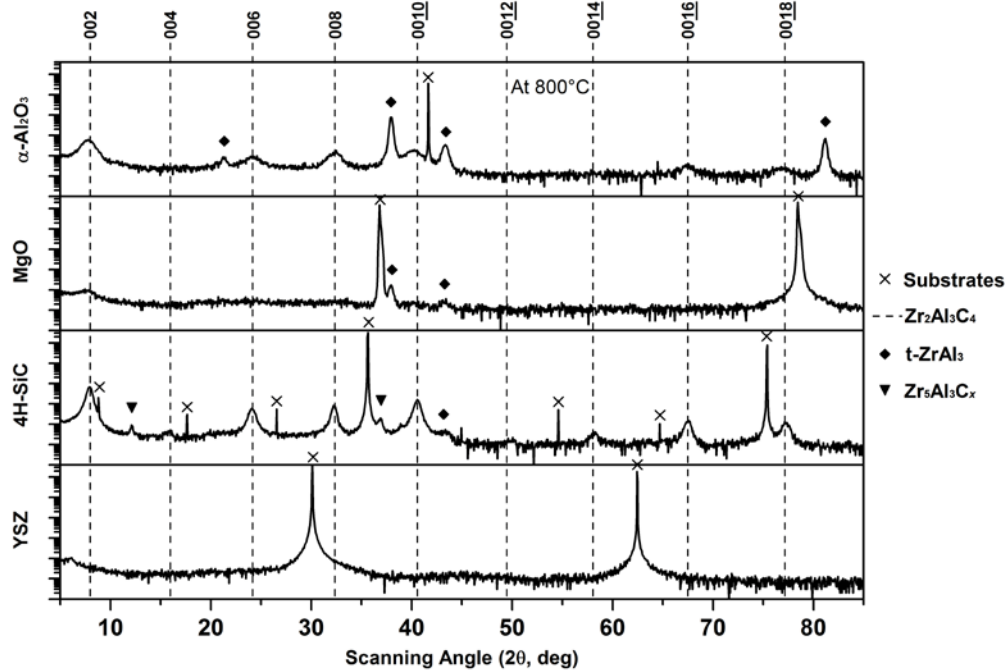
Fig. 4. θ–2θ XRD patterns of $Zr_2Al_3C_4$ grown on α-Al_2O_3(001) substrates at four different substrate temperatures, all with the incident atomic flux ratio (Al/Zr)=5.75 and (C/Zr)=1.67.

mobility and diffusion. At higher temperatures, the adatoms are supplied with more thermal energy and are more kinetically mobile, which enables diffusion into possible energetically favorable sites. Therefore comparatively long range order material can be formed, such as $Zr_2Al_3C_4$ compared to $ZrAl_3$, provided that the former phase is thermodynamically stable or metastable at the deposition temperature [37]. A similar observation has been reported in bulk synthesis of $Zr_2Al_3C_4$ phase where the $Zr_2Al_3C_4$ and $Zr_3Al_3C_5$ (another $(MC)_n(Al_3C_2)$ phase with $n = 3$) phases appear above 1160 °C and the $ZrAl_3$ phase dominates in lower temperature [20].

3.4 Effect of Substrate Material

Fig. 5 shows θ–2θ XRD patterns of samples deposited on α-Al_2O_3(001), MgO(111), 4 H–SiC(001) and YSZ(111) substrates at 800 °C with the same flux ratios (Al/Zr) = 5.75 and (C/Zr) = 1.67.

Fig. 5. θ–2θ XRD patterns of $Zr_2Al_3C_4$ grown on α-Al_2O_3(001), MgO(111), 4 H–SiC(001) and YSZ(111) substrates, all at 800 °C and with the incident atomic flux ratio (Al/Zr)=5.75 and (C/Zr) = 1.67.

Peaks from $Zr_2Al_3C_4$ are labeled with dashed lines, while substrate and competing phases are labeled in their respective peak positions [26]. A new competing phase, identified as hexagonal $Zr_5Al_3C_x$ [38], $x = 0$–1, appears on the 4 H–SiC substrate. $M_5A_3C_x$ phases are known stable in many transition element systems [37]. Several diffraction peaks from $Zr_2Al_3C_4$ can be observed on α-Al_2O_3 and 4 H–SiC; higher $Zr_2Al_3C_4$ and lower competing phase diffraction intensities are found on 4 H–SiC than on α-Al_2O_3. In contrast, only a weak $Zr_2Al_3C_4$ 002 peak can be observed on MgO, and there is no observation of $Zr_2Al_3C_4$ on YSZ substrates. This indicates a strong dependence of crystal growth on the structure of the underlying substrates.

The lattice misfits ε_L of the $Zr_2Al_3C_4$ phase on α-Al_2O_3(001), MgO(111), 4 H–SiC(001) and YSZ(111) substrates can be calculated by inserting the in-plane lattice constant of the film a_f and

12

the substrate a_s into the equation $\varepsilon_L = (a_f/a_s - 1) \times 100\%$. The lattice misfit to the substrate is +21.45% (sapphire), +12.08% (MgO), +8.69% (SiC) and −8.14% (YSZ), given the lattice constant $a_{Zr2Al3C4} = 3.34$ Å, $a'_{sapphire} = 2.75$ Å, $a_{MgO} = 2.98$Å, $a_{SiC} = 3.07$ Å and $a_{YSZ} = 3.63$ Å [26]. The $a'_{sapphire}$ is equal to $a_{sapphire}/\sqrt{3}$, for lattice constant matching in the [120] direction with $a_{sapphire} = 4.76$ Å; while a_{YSZ} is an averaged value from in-plane XRD analysis of 10 YSZ substrates. Though α-Al$_2$O$_3$(001) has a relatively large lattice misfit, a domain matching epitaxy (DME) can reduce the misfit significantly down to −0.6% by matching 5 Zr$_2$Al$_3$C$_4$ lattices with 6 Al$_2$O$_3$ lattices (5/6). Therefore the Zr$_2$Al$_3$C$_4$ phase can nucleate and grow on Al$_2$O$_3$ substrate. Narayan and Larson has demonstrated DME of ZnO on α-Al$_2$O$_3$(001), where the TEM image shows a 5/6 or 6/7 DME at the interface by inserting extra dislocations [39]. DME may also occur on 4 H–SiC(001) substrate with a 11/12 or 12/13 matching, which would give a misfit of less than 0.4%. However, despite the low DME misfit, the direct lattice misfit still affects the quality of thin films, where a lower lattice misfit (such as for SiC) gives improved crystal quality and higher phase purity, as shown in Fig. 5.

No trace of Zr$_2$Al$_3$C$_4$ was found in the films grown on MgO and YSZ substrates, despite a smaller misfit compared to α-Al$_2$O$_3$, indicating that the growth of the ternary phase is not solely determined by lattice matching. The condition of the substrate surface, e.g. crystal quality, roughness and surface reconstruction, can also affect film growth [40]. Usually, the surface quality of a cubic crystal cut in the [111] direction, such as MgO(111) and YSZ(111), is lower than for hexagonal and rhombohedral crystals cut in the [001] direction, due to inherent difficulties in cutting with high precision. Therefore a relatively high roughness and a high step density can easily be formed, along with an offset between [111] of the crystal and the polished surface normal. In addition, the MgO(111) surface is known for a very stable $(\sqrt{3} \times \sqrt{3})R30°$ reconstruction when O-terminated [41], which may not be completely removed after 15 min of heat treatment at 800 °C before the

deposition. If so, the $Zr_2Al_3C_4$ crystals were not grown on a bulk MgO(111) surface, but a less homogeneously reconstructed surface. On the contrary, α-Al_2O_3 and 4 H–SiC substrates are generally of higher crystal quality and precisely cut surface, which favors the nucleation and growth of thin films.

4. Conclusions

In this work epitaxial $Zr_2Al_3C_4$ thin films have been synthesized with pulsed cathodic arc, resulting in highly phase pure material on 4 H–SiC substrates. These films will allow future exploration of properties of the $Zr_2Al_3C_4$. By optimizing the deposition parameters, it is possible to pursue $Zr_2Al_3C_4$ thin films with higher phase purity by applying higher deposition temperature, supplying a higher Al flux ratio, and by using substrates with less lattice misfit. Also, despite flux ratios corresponding to the Zr_3AlC_2 MAX phase composition were tested, no trace of this phase was observed.

$Zr_2Al_3C_4$ thin film synthesis being very sensitive to flux composition, substrate temperature, and choice of substrate, is very similar to reported thin film synthesis of MAX phases. The similarities in their growth behaviors regarding A-element supersaturation and binary transition metal carbide intergrowth indicate a close relation between the two families of phases, despite the very different bonding environments of their A elements. Previously, there has been no M–element in a M–Al–C system reported for which both the MAX phase and $(MC)_n(Al_3C_2)$ or $(MC)_n(Al_4C_3)$ phase exist. However, we note that the Zr_3AlC_2 MAX phase was reported [42] in parallel with the present work.

14

References

[1] W. S. Williams, Transition-Metal Carbides, *Prog. Solid State Chem.* 6 (1971) 57-118.

[2] L. Toth, Transition Metal Carbides and Nitrides, Academic Press Inc., New York, USA, 1971.

[3] C. M. Fernandes and A. M. R. Senos, Cemented carbide phase diagrams: A review, *Int. J. Refract. Met. H.* 29 (2011) 405-418.

[4] U. Jansson and E. Lewin, Sputter deposition of transition-metal carbide films - A critical review from a chemical perspective, *Thin Solid Films* 536 (2013) 1-24.

[5] D. J. Tallman, B. Anasori, and M. W. Barsoum, A Critical Review of the Oxidation of Ti_2AlC, Ti_3AlC and Cr_2AlC in Air, *Mater. Res. Lett.* 1 (2013) 115-125.

[6] X. H. Wang and Y. C. Zhou, High-Temperature Oxidation Behavior of Ti_2AlC in Air, *Oxid. Met.* 59 (2003) 303-320.

[7] H. J. Yang, Y. T. Pei, J. C. Rao, J. Th. M. De Hosson, S. B. Li, and G. M. Song, High temperature healing of Ti_2AlC: On the origin of inhomogeneous oxide scale, *Scripta Mater.* 65 (2011) 135-138.

[8] X. H. Wang and Y. C. Zhou, Oxidation behavior of Ti_3AlC_2 at 1000–1400 C in air, *Corros. Sci.* 45 (2003) 891-907.

[9] X. H. Wang, F. Z. Li, J. X. Chen, and Y. C. Zhou, Insights into high temperature oxidation of Al_2O_3-forming Ti_3AlC_2, *Corros. Sci.* 58 (2012) 95-103.

[10] L. F. He, Z. J. Lin, Y. W. Bao, M. S. Li, J. Y. Wang, and Y. C. Zhou, Isothermal oxidation of bulk $Zr_2Al_3C_4$ at 500 to 1000 °C in air, *J. Mater. Res.* 23 (2008) 359-366.

[11] P. Eklund, M. Beckers, U. Jansson, H. Högberg, and L. Hultman, The $M_{n+1}AX_n$ phases: Materials science and thin-film processing, *Thin Solid Films* 518 (2010) 1851-1878.

[12] M. W. Barsoum, The $M_{N+1}AX_N$ Phases: A New Class of Solids; Thermodynamically Stable Nanolaminates, *Prog. Solid St. Chem.* 28 (2000) 201-281.

[13] Y. C. Zhou, L. F. He, Z. J. Lin, and J. Y. Wang, Synthesis and structure–property relationships of a new family of layered carbides in Zr-Al(Si)-C and Hf-Al(Si)-C systems, *J. Euro. Ceram. Soc.* 33 (2013) 2831-2865.

[14] N. V. Tzenov and M. W. Barsoum, Synthesis and Characterization of Ti_3AlC_2, *J. Am. Ceram. Soc.* 83 (2000) 825-832.

[15] K. Fukuda, S. Mori, and S. Hashimoto, Crystal structure of $Zr_2Al_3C_4$, *J. Am. Ceram. Soc.* 88 (2005) 3528-3530.

[16] L. F. He, Z. J. Lin, J. Y. Wang, Y. W. Bao, and Y. C. Zhou, Crystal structure and theoretical elastic property of two new ternary ceramics $Hf_3Al_4C_6$ and $Hf_2Al_4C_5$, *Scripta Mater.* 2008 (2008) 679-682.

[17] L. F. He, Y. W. Bao, J. Y. Wang, M. S. Li, and Y. C. Zhou, Microstructure and mechanical and thermal properties of ternary carbides in Hf–Al–C system, *Acta Mater.* 57 (2009) 2765-2774.

[18] T. El-Raghy, A. Zavaliangos, M. W. Barsoum, and S. R. Kalidindi, Damage Mechanisms around Hardness Indentations in Ti_3SiC_2, *J. Am. Ceram. Soc.* 80 (1997) 513-516.

[19] J. C. Schuster and H. Nowotny, Investigations of the ternary systems (Zr, Hf, Nb, Ta)-Al-C and studies on complex carbides, *Z. Metallkd.* 71 (1980) 341-346.

[20] L. F. He, Z. J. Lin, J. Y. Wang, Y. W. Bao, M. S. Li, and Y. C. Zhou, Synthesis and Characterization of Bulk $Zr_2Al_3C_4$ Ceramic, *J. Am. Ceram. Soc.* 90 (2007) 3687-3689.

[21] J. Zhang, L. F. He, and Y. C. Zhou, Highly conductive and strengthened copper matrix composite reinforced by $Zr_2Al_3C_4$ particulates, *Scr. Mater.* 60 (2009) 976-979.

[22] J. Rosen, L. Ryves, P. O. Å. Persson, and M. M. M. Bilek, Deposition of epitaxial Ti_2AlC thin films by pulsed cathodic arc, *J. Appl. Phys.* 101 (2007) 056101.

[23] P. O. Å. Persson, J. Rosen, D. R. McKenzie, and M. M. M. Bilek, Formation of the MAX-phase oxycarbide $Ti_2AlC_{1-x}O_x$ studied via electron energy-loss spectroscopy and first-principles calculations, *Phys. Rev. B* 80 (2009) 092102.

[24] A. Mockute, P. O. Å. Persson, F. Magnus, A. S. Ingason, S. Olafsson, L. Hultman, and J. Rosen, Synthesis and characterization of arc deposited magnetic $(Cr,Mn)_2AlC$ MAX phase films, *Phys. Status Solidi RRL* 8 (2014) 420.

[25] M. D. Tucker, Z. Czigány, E. Broitman, L.-Å. Näslund, L. Hultman, and J. Rosen, Filtered pulsed cathodic arc deposition of fullerene-like carbon and carbon nitride films, *J. Appl. Phys.* 115 (2014) 144312.

[26] PDF 00-029-1127 (4H-SiC), PDF 00-045-0946 (MgO), PDF 00-046-1212 (Al_2O_3) in: PDF-2/Release 2010 RDB (Database), International Centre for Diffraction Data (ICDD), Newtown Square, PA, USA, 2010.

[27] PDF 01-074-9352 ($Zr_2Al_3C_4$) in: PDF-2/Release 2010 RDB (Database), International Centre for Diffraction Data (ICDD), Newtown Square, PA, USA, 2010.

[28] PDF 00-035-0784 (ZrC) in: PDF-2/Release 2010 RDB (Database), International Centre for Diffraction Data (ICDD), Newtown Square, PA, USA, 2010.

[29] M. Sillassen, P. Eklund, N. Pryds, and J. Bøttiger, Effects of dopant concentration and impurities on the conductivity of magnetron-sputtered nanocrystalline yttria-stabilized zirconia, *Solid State Ionics* 181 (2010) 864-867.

[30] Z. J. Lin, L. F. He, M. S. Li, J. Y. Wang, and Y. C. Zhou, Layered stacking characteristics of ternary zirconium aluminum carbides, *J. Mater. Res.* 22 (2007) 3058-3066.

[31] O. Wilhelmsson, J. P. Palmquist, E. Lewin, J. Emmerlich, P. Eklund, P. O. Å. Persson, H. Högberg, S. Li, R. Ahuja, O. Eriksson, L. Hultman, and U. Jansson, Deposition and characterization of ternary thin films within the Ti–Al–C system by DC magnetron sputtering, *J. Cryst. Growth* 291 (2006) 290-300.

[32] J. Emmerlich, H. Högberg, S. Sasvári, P. O. Å. Persson, L. Hultman, J. P. Palmquist, U. Jansson, Jon M. Molina-Aldareguia, and Z. Czigány, Growth of Ti_3SiC_2 thin films by elemental target magnetron sputtering, *J. Appl. Phys.* 96 (2004) 4817-4826.

[33] PDF 01-072-9258 ($ZrAl_3$) in: PDF-2/Release 2010 RDB (Database), International Centre for Diffraction Data (ICDD), Newtown Square, PA, USA, 2010.

[34] Z. Wang and X. Liu, Reaction in the $Al-ZrO_2$-C system, *J. Mater. Sci.* 40 (2005) 4727-4735.

[35] L. F. He, Y. C. Zhou, Y. W. Bao, Z. J. Lin, and J. Y. Wang, Synthesis, Physical, and Mechanical Properties of Bulk $Zr_3Al_3C_5$ Ceramic, *J. Am. Ceram. Soc.* 90 (2007) 1164-1170.

[36] R. Zhang, G. Chen, and W. Han, Synthesis, mechanical and physical properties of bulk $Zr_2Al_4C_5$ ceramic, *Mater. Chem. Phys.* 119 (2010) 261-265.

[37] A. I. Gusev, Phase equilibria in M-X-X' and M-Al-X ternary systems (M = transition metal; X, X' — B, C, N, Si) and the crystal chemistry of ternary compounds, *Russ. Chem. Rev.* 65 (1996) 379-419.

[38] PDF 03-065-2033 (Zr_5Al_3) in: PDF-2/Release 2010 RDB (Database), International Centre for Diffraction Data (ICDD), Newtown Square, PA, USA, 2010, vol. Newtown Square, PA, USA.

[39] J. Narayan and B. C. Larson, Domain epitaxy: A unified paradigm for thin film growth, *J. Appl. Phys.* 93 (2003) 278-285.

[40] J. L. Schroeder, A. S. Ingason, J. Rosen, and J. Birch, Beware of poor-quality MgO substrates: A study of MgO substrate quality and its effect on thin film quality, *J. Cryst. Growth* 420 (2015) 22-31.

[41] R. Plass, K. Egan, C. Collazo-Davila, D. Grozea, E. Landree, L. D. Marks, and M. Gajdardziska-Josifovska, Cyclic Ozone Identified in Magnesium Oxide (111) Surface Reconstructions, *Phys. Rev. Lett.* 81 (1998) 4891-4894.

[42] T. Lapauw, J. Halim, J. Lu, T. Cabioc'h, L. Hultman, M.W. Barsoum, K. Lambrinou, J. Vleugels, Synthesis of the novel Zr_3AlC_2 MAX phase, *J. Eur. Ceram. Soc.* (2015).